

Effects of angular momentum projection on the nuclear partition function and the observation of the giant dipole resonance in hot nuclei

W.E. Ormand^{a,b,c}, P.F. Bortignon^a, R.A. Broglia^{a,d}

^a*Dipartimento di Fisica, Università di Milano, and Istituto Nazionale di Fisica Nucleare sezione di Milano, Via Celoria 16, 20133 Milano, Italy*

^b*Physics Division, Oak Ridge National Laboratory, P.O. Box 2008, MS-6373 Building 6003, Oak Ridge, TN 37831-6373 USA*

Louisiana State University, Baton Rouge, LA 70803-4001

^d*The Niels Bohr Institute, University of Copenhagen, Blegdamsvej 17, DK-2100 Copenhagen Ø, Denmark*

Abstract

Procedures for projecting angular momentum in a model describing a hot nucleus that takes into account large-amplitude quadrupole fluctuations are discussed. Particular attention is paid to the effect angular-momentum projection has on the observables associated with the γ -decay of the giant-dipole resonance (GDR). We also elaborate on which of the different projection methods provides the best overall description of the GDR, including angular distributions. The main consequence of angular-momentum projection is the appearance of an effective volume element in the integrals associated with the thermal average of the physical observables. This effective volume element is controlled by the value of the moments of inertia of the system. In the limit of rigid-body moments of inertia, the effective volume element is found to differ only slightly from the volume element associated with the normalization of the five-dimensional quadrupole oscillator wavefunction in the β, γ ,

and Ω space, namely $\mathcal{D}[\alpha] = \beta^4 d\beta \sin(3\gamma) d\gamma d\Omega$. In the limit of irrotational flow moments of inertia, the leading behavior in the β degree of freedom is $\mathcal{D}[\alpha] \propto \beta d\beta$.

PACS numbers: 21.10.-k, 21.60.Ev

I. INTRODUCTION

It is well known that when a nucleus is observed at finite excitation energy, large-amplitude thermal fluctuations can play an important role. An example is provided by the cross section of the giant-dipole resonance (GDR) in a hot nucleus [1–3], which may be written as a weighted average over the deformation parameters $\alpha_{\lambda\mu}$,

$$\sigma(E) = Z^{-1} \int \mathcal{D}[\alpha] \sigma(\alpha; E) e^{-F(T,\alpha)/T}. \quad (1)$$

Here E is the photon energy, $\sigma(\alpha; E)$ is the deformation-dependent cross section of the GDR evaluated in the laboratory frame. The quantity F represents the free energy of the system at temperature T , and

$$Z = \int \mathcal{D}[\alpha] \exp(-F/T), \quad (2)$$

is the partition function. Eq. (1) is equivalent to the single-time slice limit, or static-path approximation (SPA), of the path-integral formulation of Refs. [4,5], and should be understood as an adiabatic limit: i.e., under the assumption that the time scale for sampling the quadrupole shape deformations is long compared to the change in the dipole frequency associated with the shape fluctuations. For a description of the effects of nonadiabatic thermal fluctuations on the GDR, see Refs. [6,7].

In the case of the GDR, the strongest coupling is to the quadrupole degrees of freedom, which are defined by the quadrupole deformation parameters β and γ , and the Euler angles (ϕ, θ, ψ) ¹ defining the intrinsic orientation of the system. The volume element $\mathcal{D}[\alpha]$ has been the source of controversy in the past [1–3]. With the choices being between $\mathcal{D}^{(1)}[\alpha] = \beta^4 d\beta \sin(3\gamma) d\gamma d\Omega$ [4], with $d\Omega = \sin\theta d\theta d\phi d\psi$ and $\mathcal{D}^{(2)}[\alpha] = \beta d\beta d\gamma d\Omega$ [1,2]². The first choice

¹The Euler angles and rotation matrices are defined using the convention of Edmonds [8]. At an arbitrary orientation, the $\alpha_{2\mu}$ are given by $\alpha_{2\mu} = \sum_m a_m D_{\mu m}^2$, with $a_0 = \beta \cos \gamma$, $a_2 = a_{-2} = \beta \sin \gamma / \sqrt{2}$, and $a_1 = a_{-1} = 0$.

²In Refs. [1,2], the integration over $d\Omega$ was not performed

arises naturally in the quantization of the five-dimensional quadrupole oscillator, or Bohr Hamiltonian [9], and the static-path approximation to the nuclear partition function [4] in the limit of that the residual interaction contains only quadrupole-quadrupole terms. The second is a generalization to non-axially symmetric quadrupole deformations of the results obtained by Bertsch [10], where the number of states per unit interval of β , was found to be proportional to $d\beta$.

In this work, three methods for projecting angular momentum onto a nuclear system at finite temperature are investigated. In the standard approach, which was used in most previous theoretical studies of the GDR in hot nuclei, angular momentum is projected on average by using a constant rotational frequency, and the GDR is basically described via Eq. (1) with $\mathcal{D}[\alpha] = \mathcal{D}^{(1)}[\alpha]$. An important drawback of this method occurs at high spin, where the free energy exhibits a fission saddle-point beyond which $F \rightarrow -\infty$ and Eq. (1) is unbound. In order to overcome this difficulty in connection with the study of the Jacobi-shape phase transition, which is likely to take place for values of angular momentum close to those leading to fission, total angular momentum projection, as is outlined in the next section, was introduced in Ref. [11].

In the present work, we examine the consequences of angular momentum projection on the GDR, and conclude that it leads to an effective volume element that is determined by the moments of inertia. In the limit of rigid-body moments of inertia, the effective volume element is found to differ only slightly from $\mathcal{D}^{(1)}[\alpha]$, while in the limit of irrotational flow moments of inertia, the leading behavior in β for the effective volume element is $\beta d\beta$. The third approach discussed here is to project only the z -component of the angular momentum in the calculation of the partition function. It is found that this method leads to strength functions and full-width-at-half-maxima that are very similar to the second projection method at low spins, but it gives a better overall description of non-scalar observables, such as the angular distribution a_2 -coefficient.

The general outline of this paper is as follows. In Section II, the three methods of projecting angular momentum are derived and discussed. In Section III, the application of

projection methods to the GDR is discussed, while comparisons between the methods are shown as a function of angular momentum for the nuclei ^{106}Sn and ^{208}Pb in Section IV. Concluding remarks are given in Section V.

II. ANGULAR MOMENTUM PROJECTION METHODS

The intrinsic cross section $\sigma(\alpha; E)$ of the GDR and the free energy F are naturally evaluated in the cranking model at a fixed frequency ω , while the (external) cross section should be evaluated at a fixed angular momentum J . The transformation from frequency to angular momentum may be performed by adjusting the frequency to give the correct angular momentum value. If this is done independently for each quadrupole deformation and orientation, one is lead to use an effective volume element in Eq. (1). To see this, we begin with the partition function at fixed frequency and temperature,

$$Z(\omega, T) = \text{Tr} \left(e^{-(H-\omega J_z)/T} \right) = \int \mathcal{D}[\alpha] e^{-F(T, \alpha, \omega)/T}. \quad (3)$$

Except for a prefactor to the integral, we note that this expression is obtained in the static-path approximation to a quadrupole deformed nucleus at finite temperature [4]. The volume element is given by $\mathcal{D}[\alpha] = \mathcal{D}[\alpha]^{(1)}$ and $e^{-F(T, \alpha, \omega)/T}$ is the probability distribution at fixed frequency. The partition function for a fixed value M of the z -component of the angular momentum is given by the inverse Laplace transform with respect to the frequency

$$Z_M(T) = \text{Tr}_M \left(e^{-H/T} \right) = \frac{1}{2\pi iT} \int_{-i\infty}^{i\infty} d\omega e^{-\omega M/T} Z(\omega, T). \quad (4)$$

The partition function at fixed angular momentum J is then obtained by differentiation with respect to M via

$$\begin{aligned} Z_J(T) &= \text{Tr}_J \left(e^{-H/T} \right) = (2J + 1) [Z_{M=J}(E) - Z_{M=J+1}(E)] \\ &\approx -(2J + 1) \frac{\partial}{\partial M} Z_M(E) \Big|_{M=J+\frac{1}{2}} \\ &= \frac{2J + 1}{2\pi iT^2} \int_{-i\infty}^{i\infty} d\omega \omega e^{-\omega(J+\frac{1}{2})/T} Z(\omega, T) \\ &= \frac{2J + 1}{2\pi iT^2} \int \mathcal{D}[\alpha] \left[\int_{-i\infty}^{i\infty} d\omega \omega e^{-\left(\omega(J+\frac{1}{2})+F(T, \alpha, \omega)\right)/T} \right], \end{aligned} \quad (5)$$

In the last expression of Eq.(5), the quantity inside the square bracket may be identified with the effective probability distribution for the deformation characterized by the parameters α at fixed spin. The integration over ω is usually approximated by applying the saddle-point technique [12]. In this regard, there are two choices: the application of the saddle-point approximation before or after the integration over deformation degrees of freedom. In the latter case, the saddle-point condition is

$$J + \frac{1}{2} = T \frac{\partial}{\partial \omega} \ln Z(\omega, T) \Big|_{\omega=\omega_J}, \quad (6)$$

leading to a constant rotational frequency, ω_J , applied at all deformations, and the fixed angular momentum partition function is given by

$$Z_\omega(J, T) = \frac{(2J + 1)}{T^2 (2\pi D)^{1/2}} \omega_J e^{-\omega_J(J+1/2)/T} \int \mathcal{D}[\alpha] e^{-F(T, \alpha, \omega_J)}, \quad (7)$$

where $D = \frac{\partial^2}{\partial \omega^2} \ln Z(\omega, T) \Big|_{\omega=\omega_J}$. This approach applies a constraint so that the expectation value of the angular momentum is, on average, equal to J . As such, at higher spins, large variations in the projected angular momentum, which can be measured by computing the variance of J , can be expected.

In the case of applying the saddle-point integration before integrating over the deformation degrees of freedom, one obtains a rotational frequency, $\omega_{\alpha, J}$, for each deformation and orientation that is given by

$$J + \frac{1}{2} = - \frac{\partial}{\partial \omega} F(T, \alpha, \omega) \Big|_{\omega=\omega_{\alpha, J}}. \quad (8)$$

It is an open question as to which choice of performing the integration over ω leads to a better evaluation of the nuclear partition function, and, by extension, the expectation value of spin-dependent observables. However, we note that since the nuclear free energy is a rotational invariant, it must be at least a quadratic function of the rotational frequency. Consequently, to lowest order, the free energy may be written as

$$F(T, \alpha, \omega) = F(T, \alpha, \omega = 0) - \frac{1}{2} \omega^2 (I_1 \cos^2 \psi \sin^2 \theta + I_2 \sin^2 \psi \sin^2 \theta + I_3 \cos^2 \theta), \quad (9)$$

$$= F(T, \alpha, \omega = 0) - \frac{1}{2} \omega^2 \mathcal{I}(\beta, \gamma, \theta, \psi), \quad (10)$$

where the I_k are the nuclear moments of inertia. At this point, we note that as long as there are no quartic terms in the free energy, Eq.(5) can be evaluated analytically, and the saddle-point integral applied before the integration over the quadrupole degrees of freedom, as indicated in Eq.(8), is exact. Therefore, one may write the partition function as

$$Z(J, T) = \frac{(2J+1)^2}{2(2\pi T^3)^{1/2}} \int \frac{\mathcal{D}[\alpha]}{\mathcal{I}(\beta, \gamma, \theta, \psi)^{3/2}} \exp[-F(T, \alpha, J)/T]. \quad (11)$$

where $F(T, \alpha, J) = F(T, \alpha, \omega = 0) + (J + \frac{1}{2})^2/2\mathcal{I}(\beta, \gamma, \theta, \psi)$. Note that the saddle-point frequency of Eq. (8) corresponds to

$$\omega_{\alpha, J} = \frac{J + \frac{1}{2}}{\mathcal{I}(\beta, \gamma, \theta, \psi)}. \quad (12)$$

From Eq.(11), it is apparent that the moments of inertia define an effective volume element, $\mathcal{D}^{eff}[\alpha] = \mathcal{D}[\alpha]/\mathcal{I}(\beta, \gamma, \theta, \psi)^{3/2}$. For nuclei, there are two limiting cases for the moments of inertia that are of interest. The first being when the angular momentum is built up entirely from the collective degrees of freedom, at which point the moments of inertia would correspond to the irrotational-flow values: $I_k^{irrot} = I_0\beta^2 \sin^2(\gamma + 2\pi k/3)$, where $I_0 = (3/2\pi)MR_0^2$, and the effective volume element is proportional to $\beta d\beta$ and is given by

$$\frac{\beta d\beta \sin(3\gamma) d\gamma d\Omega}{[I_0(\sin^2(\gamma + 2\pi/3) \cos^2 \psi \sin^2 \theta + \sin^2(\gamma + 4\pi/3) \sin^2 \psi \sin^2 \theta + \sin^2(\gamma) \cos^2 \theta)]^{3/2}}, \quad (13)$$

which differs sharply from $\mathcal{D}^{(1)}[\alpha]$. Indeed, since there are shapes for which $I_k^{irrot} = 0$, there are orientations in which \mathcal{D}^{eff} diverges to infinity. These apparent divergences, however, are brought under control by a similar factor in the exponential of the free energy $\exp[-(J + \frac{1}{2})^2/2\mathcal{I}(\beta, \gamma, \theta, \psi)]$.

The second limit of interest is the case where the nuclear moments of inertia assume the rigid-body values, $I_k^{rigid} \approx I_0 [1 - \sqrt{5/4\pi}\beta \cos(\gamma + 2\pi k/3)]$ with $I_0 = (2/5)MR_0^2$. In this case, the effective volume element is similar to $\mathcal{D}^{(1)}[\alpha]$. Shown in Fig. 1 is the contour plot of $I_0^{3/2}\mathcal{D}^{eff}[\alpha]/\mathcal{D}^{(1)}[\alpha] = [I_0/\mathcal{I}(\beta, \gamma, \theta, \psi)]^{3/2}$ for rigid-body moments of inertia with Euler angles $\phi = 0$ and $\theta = \psi = \pi/4$. As can be seen in the figure, the effective volume element obtained with the rigid-body moments of inertia differs from $\mathcal{D}^{(1)}[\alpha]$ for $\beta \leq 1.0$ by at

most a factor of 2.5. This difference is not readily observable in the partition function (or observables of the GDR) for temperatures less than 2 MeV because the integral in Eq.(11) is dominated by the free energy in the exponential. In fact, for such large values of β the free energy is often larger than the minimum value by 20 MeV or more, and, consequently, is suppressed by the exponential factor.

As a further illustration of the effects of angular momentum projection, density distributions for the effective weight function $W = \mathcal{D}^{eff} \exp[-F/T]$ are plotted in Fig. 2 for the nucleus ^{106}Sn at temperatures $T = 1$ and 3 MeV and zero angular momentum for irrotational flow and rigid-body moments of inertia as well for the fixed rotational frequency (ω) method. The free energy was evaluated using the temperature-dependent liquid-drop parameterization of Guet *et al.*, which is based on finite temperature, extended Thomas-Fermi calculations [13]. In the figure, the darker shaded areas reflect the largest weight. Note that the weight functions obtained for the angular momentum projected case using rigid-body moments of inertia are very similar in shape to the fixed ω method. There is, however, an important difference. In the fixed ω method, each of the three regions have the same relative weight, whereas, in the case of projected angular momentum, the weight function is asymmetric in the three regions. This is due to an angular anisotropy in the factor $\mathcal{I}^{-3/2}(\beta, \gamma, \theta, \psi)$, which arises, in part, from fluctuations of the rotational frequency while projecting angular momentum. Although this factor essentially allows for an exact computation of the partition function at the mean field level via Eq. (11), the anisotropy in the effective volume element can have important consequences for observables of the GDR. In particular, it will be shown in the Section IV that although the total GDR strength function is essentially unaffected, the angular distribution a_2 -coefficient (defined in the next section) is, and is one motivation for using the projection method outlined below for just projecting J_z .

The nuclear moments of inertia can be evaluated from cranked Nilsson-Strutinsky calculations, which, at high temperature, tend towards the rigid-body limit. At low temperature, however, significant corrections due to shell structure and the pairing interaction may be

present, and the moments of inertia may correspond to a mixture of the two limits. In practice, however, the moments of inertia never correspond solely to the irrotational limit, as this would preclude angular momentum built up of non-collective single-particle excitations.

An important difference between these two methods of projecting angular momentum has to do with the presence of a fission barrier at finite spin. In the fixed rotational frequency scheme, there is always a saddle point in the free energy along the prolate collective axes for $\omega_{rot} > 0$. The position and height of the saddle point naturally decreases with increasing rotational frequency, as is illustrated in Fig. 3, where the free energy in the fixed rotational frequency approach is plotted for the nucleus ^{106}Sn at a temperature $T = 2.0$ MeV for rotational frequencies $\omega_{rot} = 0.0, 0.56, 1.02, \text{ and } 1.31$ MeV, which approximately correspond to angular momentum values $0, 20, 40, \text{ and } 60\hbar$, respectively.

Given the presence of the fission barrier, care must be taken when computing the partition function and accounting for the effects of large-amplitude thermal fluctuations on the GDR since beyond the saddle point the free energy decreases to $-\infty$, and from a technical point of view, the integral over all quadrupole degrees of freedom is unbound. In this case, the integration over β must be limited to values below the saddle point. On the other hand, using the method of Eq. (11), there is no saddle point in the free energy, and the integration over the quadrupole degrees of freedom is always bound. In addition, as a function of angular momentum, the mean-field nuclear shape displays three distinct characteristics instead of two as in the case of fixed rotational frequency. At low spin and temperature, the shape is governed by the ground state, equilibrium shape. For example, for a deformed nucleus, a prolate shape undergoing a collective rotation about an axis perpendicular to the symmetry axis. As the spin and temperature increase, the nucleus makes a transition to an oblate shape rotating about the symmetry axis, while at very high spins, the nucleus undergoes the Jacobi transition, which is characterized by a sudden change to a prolate shape with a very large deformation rotating about an axis perpendicular to the two symmetry axes. Note that only the first two regimes are present in the fixed rotational frequency method of projecting the angular momentum.

We conclude this section by noting that instead of projecting the total angular momentum onto the partition function via Eq. (5), it may be more appropriate in some cases to approximate total J projection with just projecting the z -component of the angular momentum, M . In this case, the partition function becomes,

$$Z_M = \frac{1}{\sqrt{2\pi T}} \int \frac{\mathcal{D}[\alpha]}{\mathcal{I}(\beta, \gamma, \theta, \psi)^{1/2}} \exp[-F(T, \alpha, M)/T], \quad (14)$$

where the free energy is given by

$$F(T, \alpha, M) = F(T, \alpha, \omega = 0) + M^2/2\mathcal{I}(\beta, \gamma, \theta, \psi), \quad (15)$$

and the saddle-point frequency is given by $\omega_{\alpha, M} = M/\mathcal{I}(\beta, \gamma, \theta, \psi)$.

III. GDR OBSERVABLES

The expectation value of a scalar observable, such as the total cross section of the giant-dipole resonance follows in a similar manner as the partition function. This is primarily because scalar observables commute with the angular momentum projection operator. In particular, the response function of the giant-dipole is proportional to the Fourier transform of the “real”-time autocorrelation function

$$\sum_i \langle i | (\sum_{\mu} d_{\mu}^{\dagger}(t) d_{\mu}(0)) e^{-\beta \hat{H}} \hat{P}_J | i \rangle, \quad (16)$$

where d_{μ} is the μ^{th} -component of the isovector dipole transition operator and \hat{P}_J is an angular momentum projection operator. Because of its high collectivity, the cross section of the GDR is often approximated by harmonic vibrations along the three principal nuclear axes with frequencies proportional to the inverse of the radius of each axis [14]. Within this framework, the cross section for the GDR is evaluated at each deformation, orientation, and rotational frequency, and is denoted by $\sigma(\alpha, \omega; E)$, and is given by Eq. (35) of Ref. [15]. The total cross section, including thermal averaging, is then

$$\sigma_J(E) = Z^{-1}(J, T) \frac{2J+1}{2\pi i T^2} \int \mathcal{D}[\alpha] \left[\int_{-i\infty}^{i\infty} d\omega \omega \sigma(\alpha, \omega; E) \exp\left(-(\omega(J + \frac{1}{2}) + F(T, \alpha, \omega))/T\right) \right]. \quad (17)$$

Approximating Eq. (17) by evaluating the dipole cross section at the saddle-point frequency for each deformation as defined in Eq. (8) leads to

$$\sigma_J(E) \approx Z^{-1}(J, T) \frac{(2J+1)^2}{2(2\pi T^3)^{1/2}} \int \mathcal{D}^{eff}[\alpha] \sigma(\alpha, \omega_{\alpha, J}; E) \exp[-F(T, \alpha, J)/T]. \quad (18)$$

In the fixed rotational frequency approach, where the rotational frequency is defined by Eq. (6), the dipole cross section is evaluated at the saddle-point frequency ω_J for each deformation and orientation, giving

$$\sigma_{\omega, J}(E) \approx Z^{-1}(\omega_J, T) \int \mathcal{D}^{(1)}[\alpha] \sigma(\alpha, \omega_J; E) \exp[-F(T, \alpha, \omega_J)/T]. \quad (19)$$

Finally, when only the z -component of the angular momentum is projected, the GDR cross section is

$$\sigma_M(E) \approx Z_M^{-1} \frac{1}{\sqrt{2\pi T}} \int \frac{\mathcal{D}^{(1)}[\alpha]}{\mathcal{I}(\beta, \gamma, \theta, \psi)^{1/2}} \sigma(\alpha, \omega_{\alpha, M}; E) \exp[-F(T, \alpha, M)/T]. \quad (20)$$

In regards to non-scalar observables, we note that much of the formalism described here is not adequate because of the fact that these observables do not commute with operators used to project the angular momentum, and it may be necessary to make further approximations.

An important non-scalar observable associated with the the giant-dipole resonance is the angular distribution a_2 -coefficient defined as

$$\sigma(E, \theta) = \sigma(E) [1 + a_2(E) P_2(\cos\theta)], \quad (21)$$

where θ is the angle between the observed GDR γ -ray and the polarized spin direction. In heavy-ion fusion experiments with high angular momenta, the z -component of the angular momentum is large ($\approx J$), and lies in a plane perpendicular to the incident beam direction. The angular distribution is often measured with the angle θ being between the observed gamma-ray and the incident beam direction. In the large J limit, the $a_2(E)$ -coefficient is given by

$$a_2(E) = \frac{1}{\sigma_{tot}(E)} \left[\sigma_0(E) - \frac{1}{2}(\sigma_1(E) + \sigma_{-1}(E)) \right], \quad (22)$$

where $\sigma_\mu(E)$ is the cross section for the μ^{th} -component of the GDR and $\sigma_{\text{tot}} = \sum_\mu \sigma_\mu$ is the total cross section. In the standard approach, each of the μ -components of the GDR strength function are computed using Eqs. (18)-(20) for each of the three projection methods, respectively.

IV. COMPARISON OF THE METHODS

In this section, we compare the results obtained with the three different projections methods as a function of temperature and angular momentum for the nuclei ^{106}Sn and ^{208}Pb . The free energies were calculated using the Nilsson-Strutinsky procedure [16,17], using the Nilsson-model and liquid-drop parameters given in Refs. [18] and [13], respectively. In addition, the moments of inertia were taken to be the rigid-body values with shell corrections applied as described in Ref. [15]. For the most part, the two nuclei are different in character, as the shell corrections in ^{106}Sn are essentially zero. This is in sharp contrast with ^{208}Pb , where strong shell corrections are present at low temperature that favor the spherical shape.

For the cross section of the giant dipole resonance, we use an extension of the quantal oscillator of Ref. [14] to include arbitrary orientations and quadrupole shapes, which is described in Ref. [15]. For a given quadrupole shape, the principal GDR modes were taken to have energy $E_k = E_0 \exp[-\sqrt{5/4\pi}\beta \cos(\gamma + 2\pi k/3)]$. Following experimental findings, the width of each mode associated with a given deformation was assumed to depend on the dipole energy by $\Gamma_k = \Gamma_0(E_k/E_0)^\delta$ [19], with $\delta = 1.8$. As in Ref. [15], the parameters E_0 and Γ_0 are taken from ground state data and are $E_0 = 14.99$ MeV and $\Gamma_0 = 5.0$ MeV for ^{106}Sn and $E_0 = 13.65$ MeV and $\Gamma_0 = 4.0$ MeV for ^{208}Pb .

Shown in Fig. 4 are the cross sections and a_2 -coefficients for the GDR in ^{106}Sn at $T = 1.6$ MeV and for $J = 0, 20, 40,$ and $60\hbar$ for the three projection methods. For the most part, the total cross section is the same for each of the three methods with the exception that at $J = 60\hbar$ the fixed ω -procedure yields a somewhat broader strength function. This is primarily due to the presence of the fission barrier, which tends to limit the range of the

integration and provides a much greater weight to larger deformations along the prolate collective axis. In regards to the a_2 coefficients, note that while the fixed ω method yields a zero value for $J = 0\hbar$, both the J - and J_z -projection methods do not, although the J_z -projection value is smaller. This rather unphysical situation is caused by the asymmetry in the weight function described in Section II and the fact that effects due to fluctuations in the rotational frequency on the GDR response function are not accounted for. On the other hand, for $J \geq 20$ all three methods give approximately the same results. This is primarily due to the fact that at higher spin, the asymmetry in the weight function is governed by the exponential factor.

By inspecting Fig. 4, one sees that the principal effects angular momentum has on the GDR are to broaden the total cross section and to enhance the a_2 -coefficient. These effects are brought about for two reasons. First, as the angular momentum increases, the minimum in the free energy shifts towards the oblate non-collective axis, and the mean deformation increases. The three μ -components then split, and as a result, the total cross section, which is the sum of all three components, broadens. For the a_2 -coefficient, not only is there a splitting caused by the mean deformation, but angular momentum causes an angular anisotropy in the weight factor, primarily through the exponential of the free energy.

Shown in Fig. 5 are the cross section and a_2 -coefficient for ^{208}Pb at $T = 1.5$ MeV for $J = 0, 20, 40,$ and $60\hbar$ for the three projection methods. As in ^{106}Sn , the three different methods give roughly the same total cross section, while the J -projection method yields a nonzero a_2 -coefficient for $J = 0\hbar$. Again all three methods yield approximately the same a_2 -coefficient for $J \geq 20\hbar$. From a comparison of Figs. 4 and 5, it is apparent that for ^{208}Pb both the width of the total cross section and the a_2 -coefficient exhibit a weaker dependence on angular momentum than for ^{106}Sn . This is primarily due to the larger moment of inertia in Pb that leads to both a smaller splitting between the μ -components of the GDR and a smaller angular anisotropy.

Another important difference between ^{208}Pb and ^{120}Sn is the influence of shell corrections. The most important of these are the shell corrections to the free energy at zero angular

momentum, which in ^{208}Pb are quite strong and tend to enhance the spherical shape at lower temperatures. In addition, because of the closed-shell structure of ^{208}Pb , shell corrections also have a strong effect on the moments of inertia. Indeed, in Ref. [15] it was found that shell corrections reduce the moment of inertia for the spherical shape by over 40% at zero temperature. Because of the $\mathcal{I}^{-3/2}$ dependence in the “effective” volume element in Eq. (11), it might be expected that the shell corrections to the moment of inertia would significantly affect the GDR strength function, as they appear to give a stronger preference to the spherical shape. We find, however, that because of the β^4 factor in the volume element, these shell corrections have very little effect on the GDR cross section beyond that produced by the free energy. This is exhibited in Fig. 6, where the weight factor (which omits the $\sin 3\gamma$ factor) $W = \beta^4/\mathcal{I}^{3/2}e^{-F/T}$ is plotted for oblate and prolate shapes at $T = 1.0$ MeV for various combinations of the shell corrections. In the top panel of the figure, the weight factor is plotted including shell corrections to the free energy as well as with and without shell corrections to the moments of inertia. The corresponding figure without shell corrections is shown in the bottom part of the figure. In both cases, it is seen that the overall behavior of the weight function is governed by the exponential of the free energy, which is plotted in the upper right-hand panel. In addition, the ratio $\mathcal{I}_{LD}/\mathcal{I}_{SHL}$ is shown in the lower left-hand panel, where it is seen that without the β^4 factor the spherical shape would have approximately 40% more weight when shell corrections to the moments of inertia are included.

At higher spins, the shell corrections to the moment of inertia in ^{208}Pb only have a moderate effect on the total GDR cross section and the a_2 -coefficient. This is despite the fact that these shell corrections significantly reduce the moment of inertia from the rigid-body value for nearly spherical shapes. The principal effect of the shell corrections would be to give to a slightly larger deformation along oblate non-collective axis in the minimum of the total free energy. Note from panel (d) in Fig. 6, however, that these shell corrections tend to damp out quickly for increasing β . On the other hand, the shell corrections to the free energy, $F(\alpha, \omega = 0)$, are quite strong, and favor the spherical shape, and, for the most

part are the dominating factor determining the influence of thermal fluctuations of the shape on the GDR. In fact, we find that at $T = 1.5$ MeV, the a_2 -coefficient obtained at $J = 60\hbar$ with and without shell corrections to the moment of inertia are essentially identical.

In regards to using purely irrotational flow moments of inertia for the calculation of the GDR properties, we note from Fig. 2 that not only due very small deformations have considerable weight, but they also have very small values for the moments of inertia. As a consequence, the saddle-point rotational frequency can be quite large (> 10 MeV), which leads to unphysical results within the model for the GDR.

To conclude this section, we note that to some degree all three methods lead to similar results with various degrees of problems in different regions. Given that the J_z -projection method can account for the Jacobi transition at high spin, whereas the fixed rotational frequency procedure cannot, and that it leads to more reasonable a_2 -coefficients for lowest values of angular momentum than does the full J -projection method, it is likely that the best all around method for describing the GDR in a hot nucleus at high spin is the J_z -projection method.

V. CONCLUSIONS

We found that the choice of the method for projecting angular momentum onto the nuclear partition function can affect the sampling of large-amplitude thermal fluctuations of the nuclear shape. In particular, angular momentum projection can lead to an effective volume element that depends on the moments of inertia of the system. We have shown that in the case of irrotational-flow moments of inertia, the effective volume element scales as $\beta d\beta$, whereas in the rigid-body limit, $\mathcal{D}^{eff}[\alpha]$ differs only slightly from the standard value of $\beta^4 d\beta \cos(3\gamma) d\gamma d\Omega$.

In practical terms, the three methods give essentially the same cross section for low to medium values of angular momentum. At higher angular momentum, the fixed rotational frequency procedure has a decreasing fission barrier that tends to favor prolate collective

shapes, but is essentially unbound, as beyond the barrier the integrand tends to infinity. In contrast, both the J - and J_z -projection methods have weight functions that are always bound and exhibit the Jacobi transition at very high spin. The primary drawback of the J -projection technique is that it fails to yield a zero valued a_2 -coefficient at $J = 0\hbar$, whereas in the J_z -projection method the a_2 -coefficient is much smaller. In conclusion, a reasonable approach to projecting angular momentum for predicting features of the giant-dipole resonance in hot nuclei is the J_z -projection method.

Acknowledgments

Oak Ridge National Laboratory is managed for the U.S. Department of Energy by Lockheed Martin Energy Research Corp. under contract No. DE-AC05-96OR22464. This work was supported in part by NSF Cooperative agreement No. EPS 9550481, NSF Grant No. 9603006, and DOE contract DE-FG02-96ER40985.

REFERENCES

- [1] M. Gallardo, M. Diebel, T. Døssing, and R.A. Broglia, Nucl. Phys. **A443**, 415 (1985).
- [2] J. M. Pacheco, C. Yannouleas, and R. A. Broglia, Phys. Rev. Lett. **61**, 1926 (1988).
- [3] Y. Alhassid, B. Bush, and S. Levit, Phys. Rev. Lett. **61**, 294 (1988); Y. Alhassid and B. Bush, Nucl. Phys. **A509**, 461 (1990).
- [4] B. Lauritzen, P. Arve, and G. F. Bertsch, Phys. Rev. Lett. **61**, 2835 (1988).
- [5] C. W. Johnson, G. H. Lang, S. E. Koonin, and W. E. Ormand, Phys. Rev. Lett. **69**, 3157 (1992).
- [6] Y. Alhassid and B. Bush, Phys. Rev. Lett. **63**, 2452 (1989).
- [7] W. E. Ormand, P. F. Bortignon, R. A. Broglia, T. Døssing, and B. Lauritzen, Phys. Rev. Lett. **64**, 2254 (1990).
- [8] A. R. Edmonds, *Angular Momentum in Quantum Mechanics* (Princeton Univ. Press, Princeton, 1960).
- [9] A. Bohr and B. R. Mottelson, *Nuclear Structure, vol. II*, (Benjamin, Reading, 1975).
- [10] G. F. Bertsch, Phys. Lett. **95B**, 157 (1980).
- [11] Y. Alhassid and N. Whelan, Nucl. Phys. **A565**, 427 (1993).
- [12] G. Arfkin, *Mathematical Methods for Physicists*, (Academic Press, New York, 1968).
- [13] C. Guet, E. Strumberger, M. Brack, Phys. Lett. **B205**, 427 (1988).
- [14] K. Neergård, Phys. Lett. **110B**, 7 (1982).
- [15] W. E. Ormand, P. F. Bortignon, R.A. Broglia, and A. Bracco, Nucl. Phys. **A** (in press).
- [16] V. M. Strutinsky, Yad. Fiz. **3**, 614 (1966) [Sov. J. Nucl. Phys. **3**, 449 (1966)]; Ark. Fys. **36**, 629 (1966); Nucl. Phys. **A95**, 420 (1967); Nucl. Phys. **A122**, 1 (1968).

- [17] M. Brack and P. Quentin, Nucl. Phys. **A361**, 35 (1981).
- [18] S. G. Nilsson, C. F. Tsang, A. Sobiczewski, Z. Szymański, S. Wycech, C. Gustafson, I.-L. Lamm, P. Möller, and B. Nilsson, Nucl. Phys. **A131**, 1.
- [19] P. Carlos *et al.*, Nucl. Phys. **A219**, 61 (1974).

FIGURES

FIG. 1. Contour plot of the effective volume element $\mathcal{D}^{eff}[\alpha]$ normalized by the factor $\mathcal{D}^{(1)}[\alpha]/I_0^{3/2}$ as a function the deformation parameters β and γ for the Euler angles $\phi = 0$, and $\theta = \psi = \pi/4$. The radius $\beta = 1$ is indicated by the dashed line, and the special values of γ denoting oblate-noncollective ($\gamma = \pi/3$), prolate collective ($\gamma = 0$), oblate collective ($\gamma = -\pi/3$), and prolate noncollective ($\gamma = -2\pi/3$) rotations are labeled.

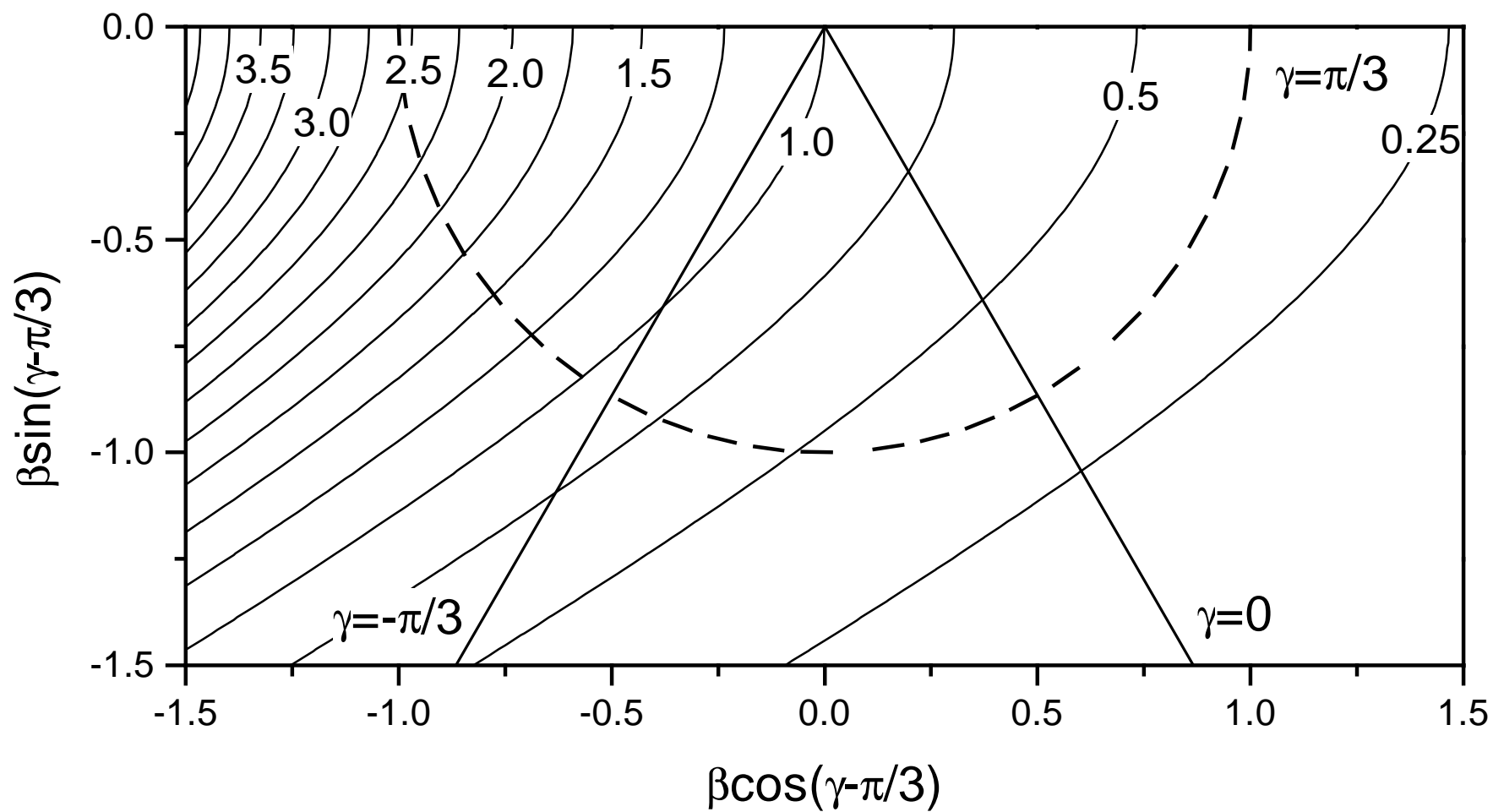
FIG. 2. Density distributions of the effective weight factor $W = \mathcal{D}^{eff}[\alpha] \exp[-F/T]$ as a function of the deformation parameters β and γ for the nucleus ^{106}Sn at temperatures $T = 1.0$ and 3.0 MeV and zero angular momentum for irrotational-flow (top panels) and rigid-body (middle panels) moments of inertia. In the bottom panels, the density distributions obtained with the fixed rotational frequency projection method assuming rigid-body moments of inertia are plotted.

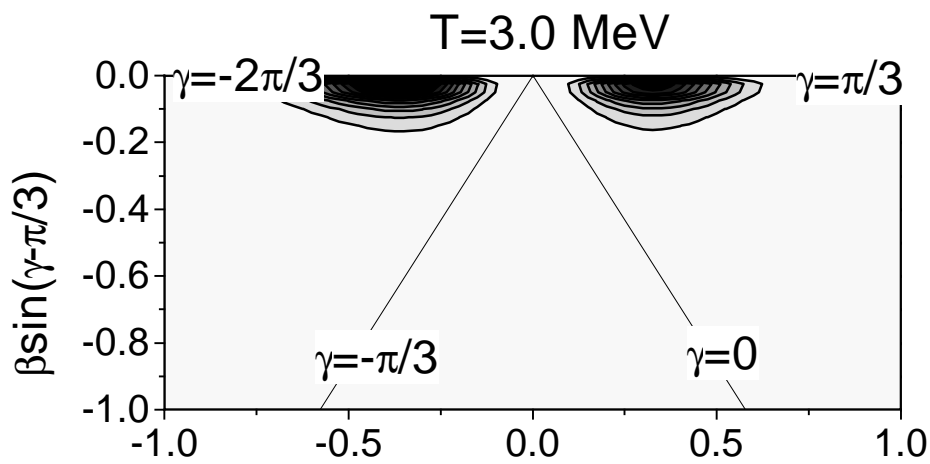
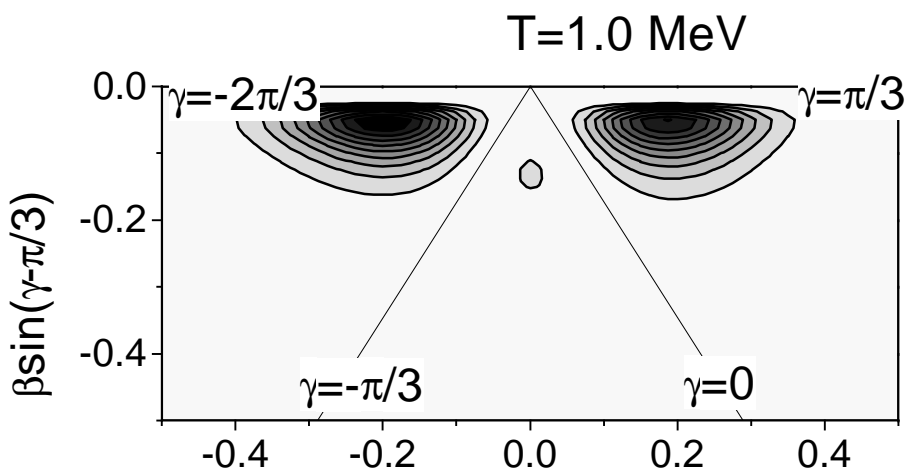
FIG. 3. The free energy for ^{106}Sn is plotted (lower panel) along the oblate noncollective ($\beta < 0$) and prolate collective ($\beta > 0$) axes at a temperature of 2 MeV and a rotational frequency of 1.25 MeV ($\langle J \rangle \approx 55\hbar$). In the upper panel, the Boltzman weight factor $\exp[-(F - F_{eq})/T]$, where F_{eq} is the minimum of the free energy below the saddle point, is plotted.

FIG. 4. Comparison between the different methods of angular momentum projection for the cross section and a_2 -coefficients for the GDR in ^{106}Sn at $T = 1.6$ MeV and $J = 0$ (solid line), 20 (dashed line), 40 (dotted line), and 60 (dot-dashed line).

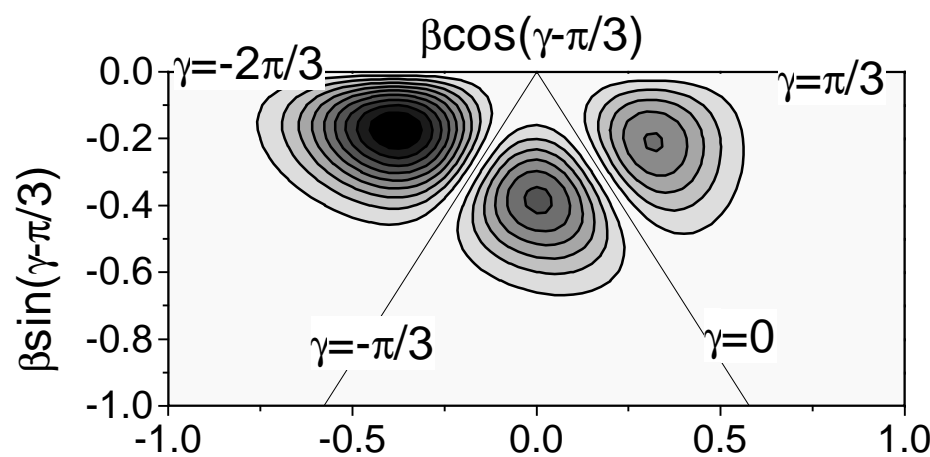
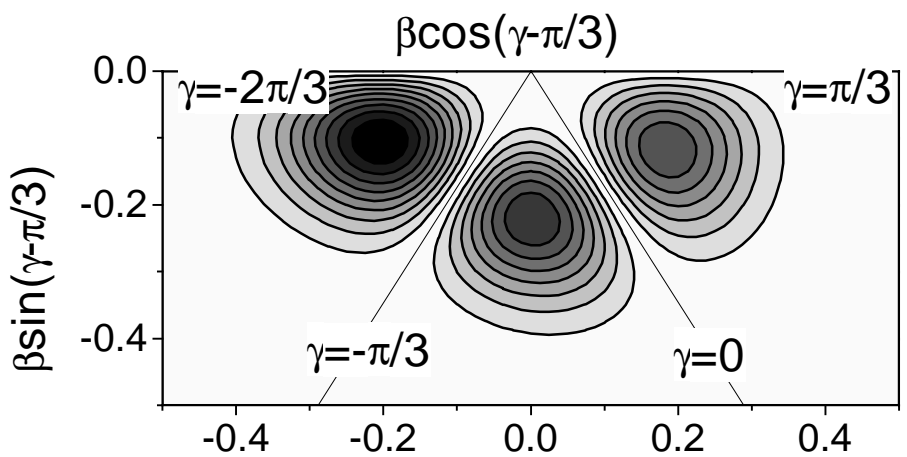
FIG. 5. Comparison between the different methods of angular momentum projection for the cross section and a_2 -coefficients for the GDR in ^{208}Pb at $T = 1.6$ MeV and $J = 0$ (solid line), 20 (dashed line), 40 (dotted line), and 60 (dot-dashed line).

FIG. 6. The weight function $W(\beta) = \beta^4/\mathcal{I}^{3/2}e^{-F/T}$ at $T = 1.0$ MeV for prolate ($\beta > 0$) and oblate ($\beta < 0$) shapes. In panel (a), $W(\beta)$ includes shell corrections to the free energy, F_{SHL} , as well as with (dotted line) and without (solid line) shell corrections to the moments of inertia. In panel (b), the same quantities are plotted without shell corrections to the free energy, i.e., $F = F_{LD}$. The free energy with and without shell corrections is plotted in panel (c), and the factor $(\mathcal{I}_{LD}/\mathcal{I}_{SHL})^{3/2}$ is plotted in panel (d).

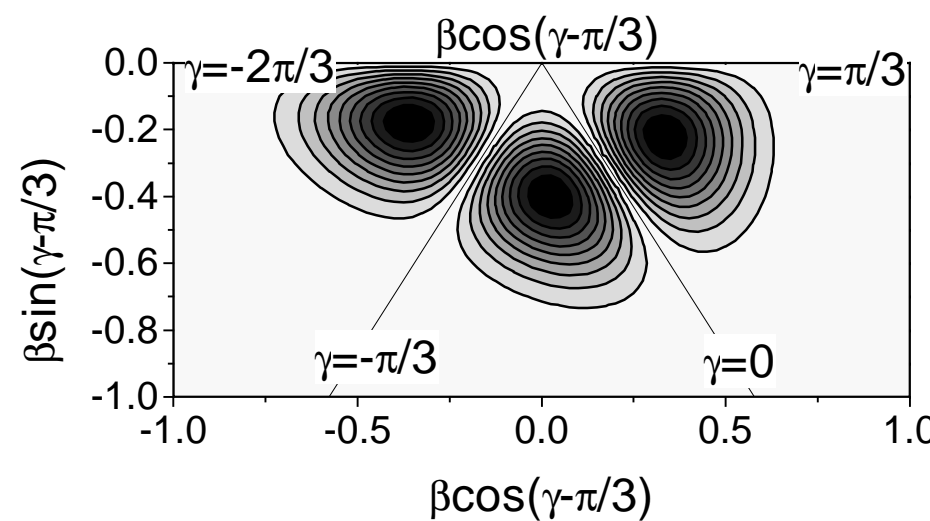
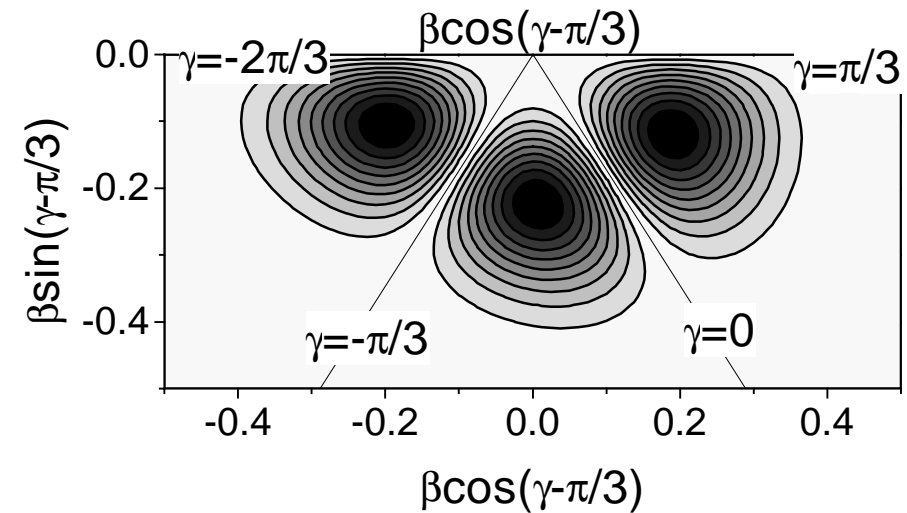




Irrotational Flow



Rigid-body



Fixed ω

